Appl Magn Reson (2015) 46:741–748
DOI 10.1007/s00723-015-0676-1

Applied
Magnetic Resonance

EPR Evidence of Unusual Dopant Valency States in Nanocrystalline Er-doped CeO_2

R. M. Rakhmatullin[1] · L. K. Aminov[1] · I. N. Kurkin[1] · A. Pöppl[2]

Received: 13 March 2015 / Published online: 5 April 2015

Abstract The structure and oxidation state of the Er dopant cation in CeO_2 single crystal and nanocrystals with size ranging from 22 to 300 nm are studied using electron paramagnetic resonance (EPR) spectroscopy at X- and at Q-band near liquid-He temperatures. Besides the expected EPR line due to Er^{3+} in cubic sites in the lattice, unusual EPR lines with g values around 14 and 20 are observed in nanocrystalline CeO_2. The appearance of these lines suggests the formation of non-Kramers Er^{2+}, Er^{4+} ions, which becomes increasing favorable with decreasing nanoparticle size. Formation of rare earth ions with such unusual oxidation states in nanoparticles can be exploited in tuning their catalytic activity and optical properties.

1 Introduction

Ceria (CeO_2) doped with trivalent cations (e.g. rare earths, Y^{3+}, Sc^{3+}) is a promising material for solid electrolytes in solid oxide fuel cells (SOFCs) [1]. Doping with trivalent cations introduces oxygen vacancies in ceria and results in fast oxygen-ion conduction via thermally activated oxygen/vacancy hopping. Some of the highest ionic conductivities are observed in Gd^{3+}- and Y^{3+}-doped ceria [2] while Er^{3+}- and Yb^{3+}-doped ceria is known for the lowest conductivity among rare earth dopants [3]. The origin of this dependence on the nature of the dopant has remained unclear since the ionic radii of some of these trivalent cations are quite similar. For example, the ionic radii of Er^{3+} and Y^{3+} in eightfold coordination with oxygen in the fluorite lattice of ceria are 1.00 and 1.01 Å, respectively [4].

✉ R. M. Rakhmatullin
rrakhmat@kpfu.ru

[1] MRS Laboratory, Kazan Federal University, Kremlevskaya 18, 420008 Kazan, Russia

[2] Faculty of Physics and Earth Sciences, University of Leipzig, Linnéstr. 5, 04103 Leipzig, Germany

Nano-structured solid electrolytes in the form of dense polycrystalline thin films and bulk ceramics with the size of the crystallites or grains being $\leq$50 nm have recently been suggested to be an effective strategy for enhancing ionic and electronic transport properties [5–7]. "Size effects" on transport in polycrystalline ionic conductors [8–14] can be expected to arise generally as consequences of interface-controlled mechanisms, associated with, e.g., the formation of extended strain fields, composition gradients and space-charge layers [10–17]. Recent studies have also indicated the existence of large differences in dopant ion coordination environments and hence in the oxygen-vacancy ordering between micro- and nanocrystalline-doped ceria of same chemical composition [18, 19]. Such structural differences are also expected to strongly influence the oxygen-ion transport and electrical conductivity in micro- vs. nanocrystalline-doped ceria.

Previous electron paramagnetic resonance (EPR) spectroscopic studies showed that rare earth ions occupy cubic and axially symmetric sites in bulk crystalline ceria [20, 21]. Evidence for some interstitial contribution was also noted for dopant cations such as Yb^{3+} and Er^{3+} in ceria [22]. Recently, we published results of the optical and microwave study of erbium-doped nanocrystalline ceria with a brief EPR part related to the cubic rare earth sites [23]. In this report, we present the results of a more detailed EPR spectroscopic study of the Er dopants in crystalline CeO_2 in the form of nanocrystalline powders with crystallite size ranging from 22 to 300 nm as well as of a single crystal ($\sim$2 mm). The effect of crystallite size on the symmetry of the coordination environment around Er and its electronic state is investigated and the possible implications of these results on the catalytic properties of these materials are discussed.

2 Experimental

2.1 Sample Synthesis and Characterization

The CeO_2 single crystal doped with Er^{3+} was grown at the Institute of Silicate Chemistry of the Russian Academy of Sciences, Saint-Petersburg, using the solution growth technique. The nanocrystalline ceria samples with 0.01 at % Er were synthesized via a co-precipitation method where an aqueous solution of NH_4OH was added dropwise to an aqueous solution containing the stoichiometric amounts of metal nitrates. The precipitated oxides were collected by centrifugation and were washed with water, a 50 % vol. ethanol–water solution and subsequently with pure ethanol. The resulting nanopowders were then dried at 120 °C for 12 h, ground and finally annealed under air at 700 °C for 2 h to obtain crystallites with diameter of $\sim$22 nm. Samples with larger grain size ($\sim$300 nm in diameter) were obtained from the nanocrystalline powders that were pelletized via cold isostatic pressing at 250 MPa and subsequently sintered at 1300 °C for 2 h. We designate hereafter the nanocrystalline powder with crystallite diameters of $\sim$22 nm as Sample 1 and that with crystallite diameter of $\sim$300 nm as Sample 2. Powder X-ray diffraction (XRD) measurements (Scintag XDS-2000) indicated that all Er-doped ceria samples studied here were characterized by the cubic fluorite crystal structure. The crystallite

size of Sample 1 was estimated from the widths of the four strongest peaks in the XRD patterns using the Williamson–Hall analysis. The particle size of Sample 2 was determined using field-emission scanning electron microscopy (SEM model FEI XL30-SFEG).

2.2 EPR Spectroscopy

The EPR spectroscopic measurements were carried out on powder samples at temperatures ranging between 10 and 11 K using continuous wave (cw) spectrometers operating at ~9.4 GHz (X-band, Bruker ESP-300) and at ~34.0 GHz (Q-band, Bruker EMX). Cryogenic temperatures were obtained using a commercial liquid-helium cryostat system (Oxford Instruments). The modulation frequencies at X-band and Q-band were 100 and 70 kHz, respectively. A Bruker dual-mode resonator (ER4146DM) designed for the investigation of forbidden EPR transitions was used for experiments in parallel mode at X-band. The cavity used had two modes: TE_{102} with B_1 perpendicular B_0 at an operating frequency of 9.6 GHz and TE_{012} with B_1 parallel to B_0, operating at a frequency of 9.3 GHz.

3 Results and Discussion

The X-band EPR spectrum of the Er-doped ceria single crystal (Fig. 1) displays the most intense EPR line corresponding to the cubic site with $g = 6.76$ due to the even isotopes and 8 relatively weak lines corresponding to the hyperfine splitting from the odd isotope Er^{167} (abundance 22.9 %) with nuclear spin $I = 7/2$, with one of them overlapping with the intense even isotopes line. Besides these, some weak lines due to the axial (trigonal) sites can also be observed in this spectrum [23, 24]. In contrast, the EPR spectra of the nanocrystalline powder samples show additional lines at effective g-factors near $g \sim 14$ and ~ 20 (we shall further designate these lines as B and A, consequently), besides the most intense line corresponding to the expected cubic spectrum of eightfold coordinated Er^{3+} ions with $g \sim 6.7$ (Fig. 1). It is worth noting here that manual grinding of the single-crystal sample does not lead to the appearance of lines A and B. Therefore, these lines must be inherently related to the nanocrystalline nature of samples 1 and 2. The larger widths ΔB_{pp} of the EPR lines of the erbium center in the nanocrystals compared to those in the single crystal imply larger degree of local structural disorder in the former that increases with decreasing crystallite size. For example, the ΔB_{pp} values for the cubic center at X-band and at 10 K are 0.20, 4.81 and 5.43 mT, respectively, for the single crystal, Sample 2 and Sample 1. At Q-band, these values are larger: 6.9 and 11.9 mT for Sample 2 and Sample 1, respectively.

The concentration of the Er^{3+} cubic centers as estimated from the EPR spectra in Fig. 1 is ~0.005 at% for Sample 2 and ~0.002 at% for the Sample 1. The concentrations of cubic sites were determined by comparing intensities of EPR lines of studied samples with the reference sample according to the method described in the work [25]. These concentrations are significantly smaller than the nominal concentration of Er of 0.01 at% in these samples. This result indicates the presence

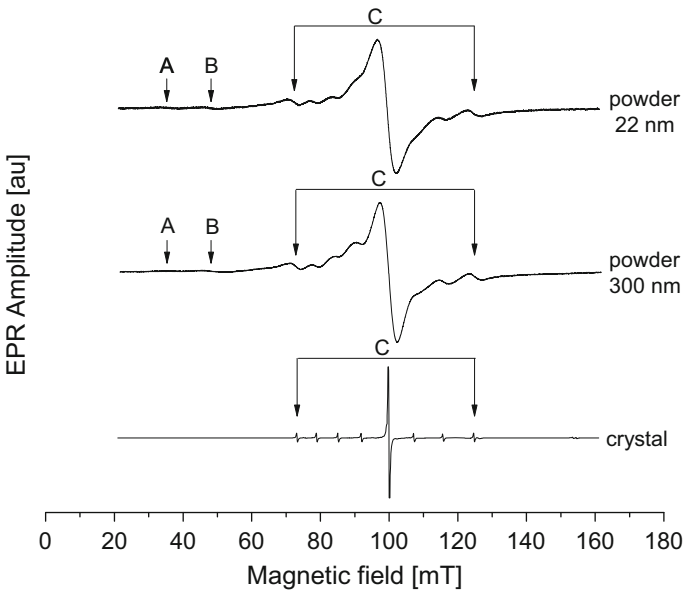

Fig. 1 X-band EPR spectra at 10 K of Er-doped CeO_2 single-crystal (*bottom*) and nanocrystalline powder samples 1 (*top*) and 2 (*middle*) with average crystallite diameters of ~22 nm and ~300 nm, respectively. The line marked by C represents the cubic center with $g = 6.76$ along with arrows marking the spread of hyperfine lines from the odd isotope Er^{167}. The weak lines marked by A and B in the spectra of samples 1 and 2 are located near $g \sim 20$ and 14, respectively

of other types of Er centers that are uniquely characteristic of the nanocrystalline ceria samples and the concentration of these centers increases with decreasing crystallite size. These unique Er centers may correspond to the "low field" lines at effective $g \sim 14$ and ~ 20 that are weak but are observed in both nanocrystalline Samples 1 and 2. Low-field EPR spectra of these two samples are collected at Q-band and compared with those collected at X-band in Fig. 2. It is clear that the intensities of the A and B lines in Fig. 2 depend on the size of the crystallites; the intensity ratio of the EPR lines at $g \sim 20$ and at $g \sim 14$ increases considerably with decreasing crystallite size. Moreover, the experimental ΔB_{pp} values for these lines increase significantly with increasing frequency of measurement. These values along with more accurate effective g values and experimental conditions are given in Table 1.

The line at $g \sim 14$ is somewhat close to a "half field line" of the cubic site and one could assign it tentatively to clustering and Er–Er pair formation. However, such an assignment is not plausible especially at the low dopant concentration where pair formation is highly unlikely. The other alternative could be the formation of low-symmetry Er^{2+}, Er^{4+} centers in the lattice. In this case, Er^{2+} should be isoelectronic to Tm^{3+} with the ground state $^3H_6$ and a Landè factor $\Lambda = 7/6$, for which the maximum possible g value for non-Kramers doublet or two close singlets is indeed $g_{\|} = 2\Lambda 6 = 14$. It may be noted that EPR spectra of Tm^{3+} with $g \sim 14$ have been observed in crystals and glasses in a number of previous studies [26, 27].

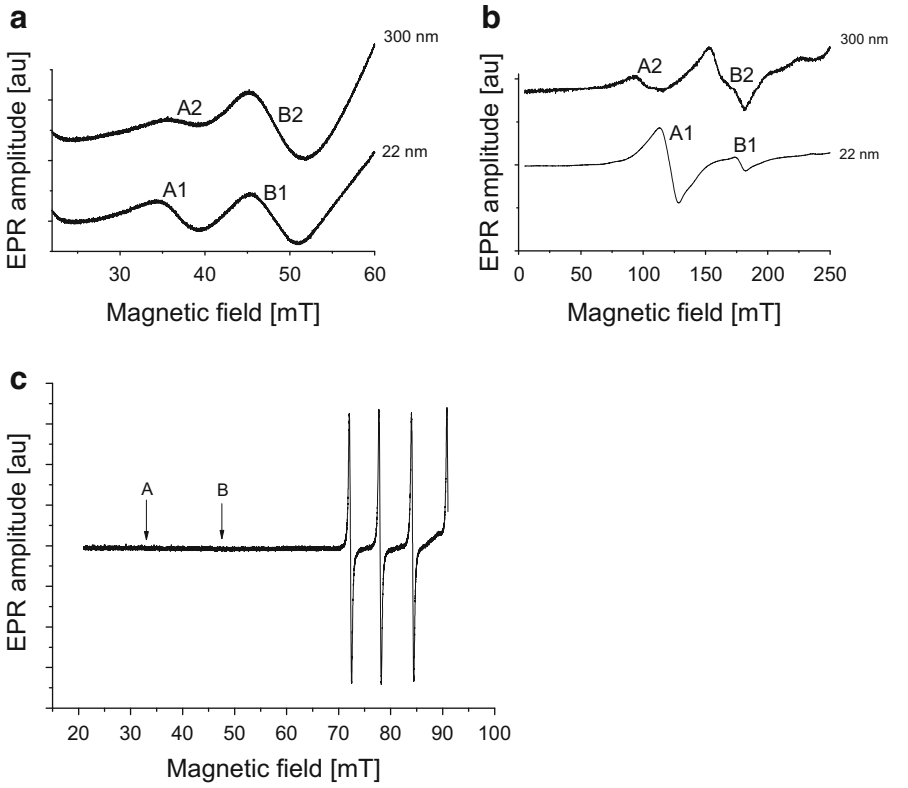

Fig. 2 Low magnetic field region of the EPR spectra of Samples 1 and 2 collected at X-band (**a**) and at Q-band (**b**). Crystallite sizes for the samples are given alongside each spectrum. The lines marked by A and B are located near $g \sim 20$ and 14, respectively. See Table 1 for precise g values and line widths for these signals. The X-band spectrum of the single-crystal sample in this magnetic field region is shown in **c**, for comparison. This spectrum is magnified by $\times 20$ to show the absence of lines A and B

Table 1 Experimental conditions and spectral parameters for the low-field EPR lines of nanoparticle samples

Sample and line	Frequency (GHz)	Temperature (K)	*g* value	Approximate linewidth (mT)
Sample 1, A	9.37	10	18.3	4.9
	34.015	9	20	16
Sample 1, B	9.37	10	13.9	5.6
	34.015	9	13.6	8
Sample 2, A	9.36	10	18	4
	33.992	9	24	22.0
Sample 2, B	9.36	10	13.8	6.5
	33.992	9	14.6	29.0

The EPR line with $g \sim 20$ could be assigned to strongly axially distorted Er^{3+} sites. It is important to note that $g = 18$ corresponds to the maximum possible value for Er^{3+} ion when the electronic wave function of the ground state ($^4I_{15/2}$) is $|\pm 15/2>$. In this case, the Landè factor $\Lambda = 6/5$ and hence $g_{||} = 2\Lambda \times 15/2 = 18$. However, in this case $g_{\perp} = 0$ and it is difficult to explain EPR observation for a Kramers ion since the magnetic dipole transitions are strictly forbidden. An alternative assignment of the EPR line with $g \sim 20$ (Fig. 2) would be to a non-Kramers Er^{4+} ion that is isoelectronic to Ho^{3+}. The ground state of Ho^{3+} is $^5I_8$, with Landè factor $\Lambda = 5/4$ that results in a maximum possible $g = 20$ for the non-Kramers doublet. The value of $g = 24$ observed for this line in Sample 2 at the Q-band can also be explained by the zero-field splitting of the non-Kramers doublet which varies slightly due to different local environments of the Er^{4+} sites. The existence of Er^{2+}, Er^{4+} sites with different zero-field splitting in the nanocrystalline samples is consistent with the fact that the lines with $g \sim 14$ and 24 in the Q-band spectrum of Sample 2 are split. This observation could be ascribed to the higher resolution of the spectra collected at Q-band compared to those collected at X-band.

It should be noted that electron spin transitions between closely situated non-magnetic singlets are possible when the static magnetic field B_0 is parallel to the microwave magnetic field and parallel to the local symmetry axis [28]. In fact in powder samples, there are always projections of both fields along the symmetry axis of paramagnetic center. We have carried out additional experiments at X-band with magnetic field B_0 parallel to the microwave magnetic field to demonstrate that the lines at $g \sim 14$ and ~ 20 do not originate from Er^{3+} Kramers centers. In this relative geometric configuration of the microwave and the static external magnetic fields, the electronic spin transitions are strictly forbidden for Kramers ions. The results for Sample 1 are shown in Fig. 3. It is clear that the main EPR line from Er^{3+} even isotopes in cubic centers has almost completely disappeared while the hyperfine lines of Er^{3+} odd isotope have become remarkably smaller compared to the lines at A and B, measured also in parallel mode. This is a strong indication that the origin of the lines at $g \sim 14$ and ~ 20 belongs to non-Kramers ions in these EPR spectra.

Here, we should note that our optical study [23] did not reveal the presence of any clustering as well as other valence state except Er^{3+} in our samples. However, the analysis of EPR spectra indicates that the concentration of centers with g values ~ 14 and ~ 20 is at least 2–3 orders less that the cubic sites. We suppose that the sensitivity of applied optical technique did not allow us to detect such small amount of erbium in other valence states.

When taken together, the results obtained in this study indicate that doping of erbium into nanocrystalline ceria is accompanied by formation of small amount of ions with valence states different from Er^{3+}. This trend is consistent with previous observations of an increased catalytic activity of ceria for driving redox reactions with decreasing crystallite size [29]. Moreover, a recent study [30] has shown that the ease with which transition metal nanoparticles change their oxidation state increases with decreasing particle size. Similar effects can be expected in rare earth oxide nanoparticles as well, and the results of this study provide strong evidence in

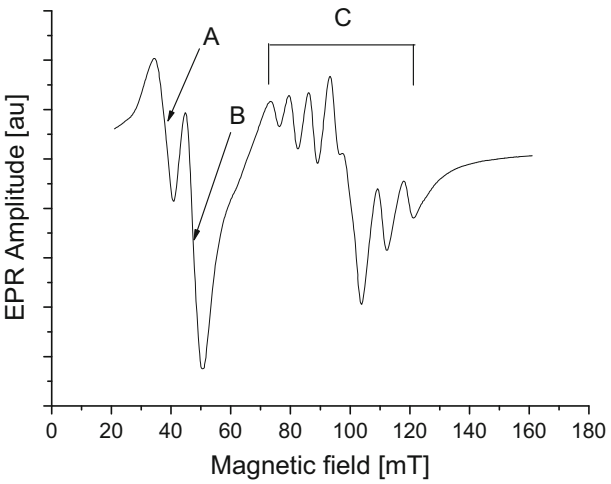

Fig. 3 EPR spectrum of Sample 1 (crystallite diameter ~22 nm) collected in parallel mode (see text for details) at X-band (9.37 GHz) and 11 K. The lines in the region marked by C are hyperfine signals from Er^{3+} odd isotopes in a cubic environment. The lines marked by A and B are the same as those in Figs. 1 and 2

favor of that hypothesis. Formation of rare earth ions with such unusual oxidation states in nanoparticles can be exploited in tuning their catalytic and optical properties that may have important implications in the areas of catalysis [31], biomarking, drug delivery [32] and photonics [33].

4 Conclusions

The EPR spectra of Er-doped CeO_2 single-crystal and nanocrystalline samples are reported. The single-crystal sample contains Er^{3+} ions in predominantly cubic sites in the fluorite structure of CeO_2. The nanocrystalline samples, on the other hand, show the presence of some fraction of non-Kramers Er^{2+} and Er^{4+} ions in low-symmetry positions, in addition to the usual Er^{3+} ions in cubic sites. Moreover, the widths of all EPR lines increase with decreasing crystallite size, indicating an increasing degree of local structural disorder. The relative fraction of the non-Kramers ions increases with decreasing crystallite size from 300 to 22 nm. Rare earth ions with such unusual oxidation states in nanoparticles may result in catalytic activity suitable for future technological applications.

Acknowledgments We grateful to Professor S. Sen from University of California at Davis for providing the nanocrystalline samples. This work was partially funded by the subsidy of the Russian Government (agreement No.02.A03.21.0002) to support the Program of Competitive Growth of Kazan Federal University among World's Leading Academic Centers. R.M. Rakhmatullin is grateful to DAAD (ref.325) for the support.

References

1. H. Inaba, H. Tagawa, Solid State Ionics **83**, 1 (1996)
2. B.C.H. Steele, Solid State Ionics **134**(1–2), 3 (2000)
3. S. Kuharuangrong, J. Power Sources **171**, 506 (2007)
4. R.D. Shannon, C.T. Prewitt, Acta Cryst. **B25**, 925 (1969)
5. J. Maier, Nat. Mater. **4**, 805 (2005)
6. H.L. Tuller, Solid State Ionics **131**, 143 (2000)
7. J. Schoonman, Solid State Ionics **135**, 5 (2000)
8. Y.M. Chiang, E.B. Lavik, I. Kosacki, H.L. Tuller, J.Y. Ying, Appl. Phys. Lett. **69**, 8 (1996)
9. J.H. Hwang, T.O. Mason, Z. Phys. Chem. **207**, 21 (1998)
10. S. Kim, J. Fleig, J. Maier, Phys. Chem. Chem. Phys. **5**, 2268 (2003)
11. S. Kim, J. Maier, J. Electrochem. Soc. **149**, 173 (2002)
12. A. Tschöpe, Solid State Ionics **139**, 267 (2001)
13. J.S. Lee, U. Anselmi-Tamburini, Z.A. Munir, S. Kim, Electrochem. Solid State Lett. **9**(8), J34 (2006)
14. I. Kosacki, T. Suzuki, V. Petrovski, H. Anderson, Solid State Ionics **136–137**, 1225 (2000)
15. J. Maier, Prog. Solid State Chem. **23**, 171 (1995)
16. J. Maier, *Physical Chemistry of Ionic Materials: Ions and Electrons in Solids* (Wiley, Chichester, 2004), p. 538
17. H.J. Park, S. Kim, J. Phys. Chem. B **111**, 14903 (2007)
18. S. Sen, H. Avila-Paredes, S. Kim, J. Mat. Chem. **18**, 3915 (2008)
19. P. Jain, H.J. Avila-Paredes, C. Gapuz, S. Sen, S. Kim, J. Phys. Chem. C **113**, 6553 (2009)
20. M.M. Abraham, R.A. Weeks, G.W. Clark, C.B. Finch, Phys. Rev. **148**, 350 (1966)
21. R.M. Rakhmatullin, L.K. Aminov, I.N. Kurkin, R. Böttcher, A. Pöppl, H. Avila-Paredes, S. Kim, S. Sen, J. Chem. Phys. **131**, 124515 (2009)
22. S.-J. Hong, A.V. Virkar, J. Am. Ceram. Soc. **78**, 433 (1995)
23. R.M. Rakhmatullin, I.N. Kurkin, V.V. Pavlov, V.V. Semashko, Phys. Status Solidi B **251**, 1545 (2014)
24. M.M. Abraham, R.A. Weeks, G.W. Clark, C.B. Finch, Phys. Rev. **148**, 350 (1966)
25. J.P. Wolfe, C.D. Jeffries, Phys. Rev. B **4**, 731 (1971)
26. E.A. Harris, D. Furniss, J. Phys.: Condens. Matter **3**, 1889 (1991)
27. J.B. Gruber, E.A. Karlow, D.N. Olsen, Phys. Rev. B **2**, 49 (1970)
28. A. Abragam, B. Bleaney, *Electron Paramagnetic Resonance of Transition Metal Ions*, (Clarendon, Oxford, 1970) pp.292-295, pp.732-736
29. S. Deshpande, S. Patil, S.V.N.T. Kuchibhatla, S. Seal, Appl. Phys. Lett. **87**, 133113 (2005)
30. A. Navrotsky, C. Ma, K. Lilova, N. Birkner, Science **330**, 199 (2010)
31. A.-W. Xu, Y. Gao, H.-Q. Liu, J. Catalysis **207**, 151 (2002)
32. W. Wang, D. Shi, J. Lian, Y. Guo, G. Liu, L. Wang, R.C. Ewing, Appl. Phys. Lett. **89**, 183106 (2006)
33. D. Matsuura, Appl. Phys. Lett. **81**, 4526 (2002)